

Coherence-induced population redistribution in optical pumping

Y. Nafcha and M. Rosenbluh

Resnick Institute for Advanced Technology and Department of Physics, Bar-Ilan University, Ramat-Gan 52900, Israel

P. Tremblay

Centre d'Optique, Photonique et Laser, Département de Génie Électrique, Université Laval, Québec (Québec), Canada, G1K 7P4

C. Jacques

Institute for National Measurement Standards, Time and Frequency Standards Group, National Research Council Canada, Ottawa, Ontario, Canada, K1A 0R6

(Received 30 December 1994; revised manuscript received 1 May 1995)

We present experimental and theoretical investigations of the ground-state levels of the Cs cycling transition. We show that in such multilevel nondegenerate systems, the populations of the extreme Zeeman sublevels, under optical pumping, can have asymmetric (“dispersive”) line shapes as a function of laser frequency. A density-matrix model which takes into account optical, Zeeman, and hyperfine coherences, and allows for a fluctuating laser field, correctly predicts the experimental observations. A comparison of the density-matrix model with a rate-equation model demonstrates the role of coherences in the population distribution. Investigation of the effect theoretically and experimentally for σ and π laser polarizations is presented in the paper.

PACS number(s): 42.50.Gy, 32.80.By

I. INTRODUCTION

Coherences play a crucial role in the population dynamics of optically pumped systems. Recently a number of authors [1] have addressed the creation of inversionless lasers and highly nonlinear but nonabsorbing systems through the use of coherences between Zeeman sublevels. In most real atomic systems which are amenable to experiment, the number of sublevels is large and some level of coherence can be established between almost any two sublevels of a system. The strong influence of coherences on the populations of the sublevels is well known and leads to many novel phenomena such as the cancellation of absorption, variable gain, high indices of refraction, and high nonlinearities. Population trapping due to Zeeman coherences and “dark resonances” arising from coherent trapping of the population in the lower level have been demonstrated in numerous experimental and theoretical treatments [2–5]. In general, it is difficult to exactly identify which of the coherences are responsible for the observed effects. This is due to the fact that a given coherence between any two states is in general dependent on the populations and coherences between all the other states in the system. This creates a highly complex and connected problem which cannot, in general, be simplified either theoretically or experimentally.

As a particular example, in the analysis of the laser spectroscopy of the Cs D_2 line one has to consider 48 Zeeman sublevels, ($F=3,4$ in the ground state and $F'=2,3,4,5$ in the excited state), thus forming a problem with 1176 linear differential equations. This leads to many different, interdependent, complex, coherence terms. While the effect of coherences on the overall behavior of an atomic system is very important, in dealing with such a large number of equations, it is often difficult to point to the physically important terms responsible for an observed effect. The significance of the coherence terms can be estimated, however, by comparing a

rate-equation calculation of a given system (which ignores all coherences) with a calculation which includes them through the use of the full density matrix.

In this paper we present the results of experiments which measure the population of a single ground-state Zeeman sublevel of the Cs atom when it is optically pumped at the cycling transition frequency. We also compare the results of a full density-matrix calculation [6] and rate-equation calculations with experimental results for both σ and π polarized light. We show that the quantitative analysis of the experimental results requires the density-matrix calculation, with the inclusion of the coherences. While the rate-equation calculation predicts the observed functional forms for the measured Zeeman sublevel populations [7,8], the population signals predicted by this model are orders of magnitude too low. To understand the physical origin of the observed population distributions in the sublevels, however, the rate-equation model is a useful guide.

The observed population redistribution in our experiments is not due to coherent population trapping, which has been discussed in connection with dark resonances [2–5]. For V-shaped systems such as the Cs $6S_{1/2}F=4 \rightarrow 6P_{3/2}F'=5$ cycling transition, it has been shown both theoretically [3] and experimentally [2] that there is no coherent trapping of populations in the ground-state levels. This is because the extreme m' states of the upper $F'=5$ level are each coupled to only one m state in the lower level involving only one component of the σ light [i.e., $\sigma^{(+)}$ or $\sigma^{(-)}$]. This can also be confirmed by measuring the excited-state fluorescence as a function of the magnetic field, which shows “normal” behavior without any sign of dark resonance behavior (Fig. 5 of Ref. [2]). Thus the origin of the dispersive shape is due to an additional means of population redistribution present in optical pumping of a multilevel system.

In Sec. II we describe the experimental setup and present the observations. Section III presents the density-matrix

model that was used to perform the calculation and in Sec. IV we present the much simplified rate-equation model we use to understand the physical origin of the observed effects. Section V contains a comparison of the various models with the observations and discusses some interesting predictions of the full density-matrix calculation.

II. EXPERIMENTAL OBSERVATIONS

In the experiments we measured the population of one of the extremum Zeeman sublevels of the $6S_{1/2}F=4$ ground state of atomic Cs as a function of laser frequency. Specifically, the experiment employed the Cs D_2 line cycling transition, $6S_{1/2}F=4 \rightarrow 6P_{3/2}F'=5$, at 852.1 nm, in an atomic beam. The atom-laser interaction region, where the atoms are optically pumped, takes place in the presence of a small (maximum 500 mG), variable and uniform magnetic field, the “C” field, in which each hyperfine state with quantum number F is split into $(2F+1)$ nearly degenerate Zeeman sublevels. The size of the splitting is 350 Hz/mG for the $6S_{1/2}F=4$ sublevels, and 560 Hz/mG for the $6P_{3/2}F'=5$ sublevels. The signal we detect is the flux of atoms in the atomic beam after the beam traverses a very strong inhomogeneous magnetic field. In the strong-field region the most convenient quantum basis is in terms of $|Jm_Jm_I\rangle$ instead of the $|JIFm_F\rangle$ quantum numbers used in zero field. Thus the $6S_{1/2}F=4$, $m_F=+4, \dots, -3$ states transform into the $m_J=+1/2$, $m_I=+7/2, \dots, -7/2$ states while the $6S_{1/2}F=3$, $m_F=+3, \dots, -3$ states and the $F=4$, $m_F=-4$ transform into $m_J=-1/2$, $m_I=-7/2, \dots, +7/2$ states. The force on the atoms in the atomic beam as they fly through the strong inhomogeneous field region depends on their m_J quantum number and thus the atoms are separated into two beams according to m_J . (The differences in trajectories for different I 's, in our apparatus is negligible.) The signal detected in the experiments is either of the two beams formed after the passage through the strong field. In the absence of interaction with light the number of atoms in either of these beams is stable to better than 1%. If a laser tuned to the cycling transition frequency interacts with the atoms, any change in the number of atoms detected in the $m_J=-1/2$ beam can only come about as a consequence of optical pumping, which changes the population of the $6S_{1/2}F=4$, $m_F=-4$ Zeeman sublevel. This in effect allows us to measure directly the population of a single Zeeman sublevel, the $6S_{1/2}F=4$, $m_F=-4$. A condition for the validity of this statement is that leakage to neighboring transitions can be neglected. Since these transitions are far from resonance with the laser frequency and the magnetic fields used in our observations are small, leakage in our experiments is negligible.

A measurement of the number of atoms in the $m_J=+1/2$ beam (the “plus beam”) for incident σ polarized laser light is shown in Fig. 1. When the laser is resonant with the $6S_{1/2}F=4 \rightarrow 6P_{3/2}F'=3$ and $F'=4$ transitions the “plus beam” signal decreases since the atoms excited to these levels can decay to the $6S_{1/2}F=3$ ground state and are thus lost from the “plus beam.” The resonances are essentially Doppler free, with the observed width due to a combination of natural lifetime broadening, residual divergence of the atomic beam and laser linewidth. For a laser at the

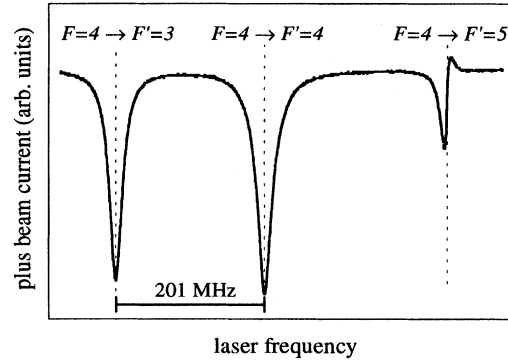


FIG. 1. The plus beam current as a function of laser frequency for typical experimental conditions: $B=200$ mG, $I=2.8$ mW/cm², σ polarization. The laser was a stabilized diode laser (SDL-5402) with feedback from a holographic grating and had a linewidth of ~ 100 kHz (FWHM). The dashed lines indicate the position of the resonances. The $F=4$ to $F'=4$ transition almost completely depletes the plus beam current to zero (defined by the frame of the figure) and the residual current is tube background current.

$6S_{1/2}F=4 \rightarrow 6P_{3/2}F'=5$ cycling transition frequency, however, the atoms can decay back only to the $6S_{1/2}F=4$ ground state and thus a signal at this transition frequency is indicative of a redistribution of populations between the Zeeman sublevels of the $F=4$ state. As shown in the figure, the cycling transition signal was found to have a “dispersive” shape as a function of laser detuning from resonance, with the dispersion centered at exact resonance. The “minus beam” in this case shows, as it should, the mirror image of the dispersive line shape. This therefore implies that the population of the $6S_{1/2}F=4$, $m_F=-4$ sublevel has a dispersive shape as a function of laser detuning from the cycling transition frequency.

The data shown in Fig. 1 were obtained with a ~ 100 kHz linewidth external cavity diode laser, but we have obtained similar results using many kinds of lasers as the source of the optical pumping, including a broad linewidth diode laser [full width at half maximum (FWHM) variable from ~ 10 MHz to ~ 30 MHz], and a stabilized ring dye laser (FWHM ~ 1 MHz). The laser linewidth influenced the amplitude of the dispersive shape and its width but the basic dispersive nature shown in Fig. 1 remained common to all the lasers. This implies that the dispersive shape of the population of the extremum Zeeman sublevels in multilevel system is a general phenomena irrespective of whether the laser linewidth is much greater (even by more than 3 orders of magnitude) or of the same order of magnitude as the Zeeman splitting of the optically pumped levels.

The experimental setup has been described previously [7] and consists of a modified Cs atomic clock tube [9] which we used in a Stern-Gerlach configuration. An oven (80°C) with an atomic beam collimator yields a Cs beam with an ~ 8 mrad divergence and a Maxwell-Boltzmann distribution of populations in the ground-state sublevels. The beam goes through a magnetically shielded region where the optical pumping is performed. The laser is introduced into this region through a small aperture hole (~ 5 mm diameter) drilled in the magnetic shield. In this shielded region we can apply a magnetic field, the “C” field, controlled by a pair of

Helmholtz coils, which determines the quantization axis. The “C” field is perpendicular to the propagation direction of the atomic beam, and the laser polarization can be aligned to be either parallel (π) or perpendicular (σ) to the field. The direction of the laser beam propagation is perpendicular to the atomic beam with an accuracy that is better than 2° . The alignment of the “C” field axis with the linearly polarized laser polarization direction (parallel or perpendicular) is maintained to within an accuracy of 5° .

Following the pumping region, at a distance of approximately 15 cm, the beam is split according to its m_j quantum number by a strong inhomogeneous separation magnet ($\langle B \rangle \sim 1.2$ T) and either the $m_j = +1/2$ or $-1/2$ beam is ionized by a hot niobium wire (wire width of 1.8 mm) and detected by an electron multiplier. For most of the data presented in this paper the laser source was a diode laser (SDL-5402) with optical feedback from a holographic grating (1800 lines/mm) in a Littrow configuration. The laser linewidth was measured by a self-beat homodyne method using a 4 km length of optical fiber. It was found to be of the order of 100 kHz. The laser beam profile was $1 \text{ mm} \times 1.7 \text{ mm}$ which for our measurements implies a $\sim 10 \mu\text{sec}$ interaction time between the atoms in the atomic beam and the laser. The niobium wire location is variable and it was positioned such that it selected atoms either from the plus or minus beam, provided they had a velocity along the atomic beam of $\sim 100 \text{ m/sec} \pm 15 \text{ m/sec}$. Such a wire position ensures that the signal-to-noise ratio remains high while only very rare, high velocity, plus (or minus) beam atoms show up in the detected minus (or plus) beam.

III. DENSITY-MATRIX MODEL

The density-matrix model is based on the semiclassical approach using the density operator formalism [10] and includes the effects of a fluctuating laser field [6]. The model corresponds closely to the actual optical pumping experiment on the cesium beam since it takes into account the effect of the atomic coherences, those of the neighboring transitions and the fact that the lasers have Lorentzian line shapes with a linewidth of the order of the natural linewidth of the cesium transitions involved. The model also includes the effect of an applied external magnetic field which modifies both the energy levels as well as the transition probabilities [12]. The diagonal elements ρ_{ii} of the density matrix ρ represent the populations of the i th levels, and the off-diagonal elements ρ_{ij} — the coherence between levels i and j . The time evolution of the density matrix obeys the analog of Liouville’s equation in classical statistical mechanics [11] to which a supplementary term, $R(t)$, has been added phenomenologically to take into account spontaneous emission and relaxation processes:

$$\frac{d}{dt} \rho(t) = \frac{1}{i\hbar} [H(t), \rho(t)] + R(t), \quad (1)$$

where $H(t)$ is the Hamiltonian which is the sum of the unperturbed Hamiltonian H_0 , and the Zeeman Hamiltonian H_Z present when an external static magnetic field \mathbf{B} is applied:

$$H_Z = \left(\frac{-\mu_B}{\hbar} \right) \mathbf{B} \cdot (\mathbf{L} + g_s \mathbf{S} + g_l \mathbf{I}), \quad (2)$$

and a term $V(t)$ describing the interaction between the atom and the optical field expressed as

$$V(t) = -\mathbf{D} \cdot \mathbf{E}(t), \quad (3)$$

where \mathbf{D} is the electric-dipole moment, and $\mathbf{E}(t)$ is the electric field of the pumping light.

The precise knowledge of the behavior of the atom under such conditions necessitates the evaluation of the energy and the state vector of each particular Zeeman sublevel [12]. Thus we must find the eigenvalues and the eigenvectors $|\Psi\rangle$ of the sum of the Hamiltonians $H_0 + H_Z$. The eigenvectors can be expressed in terms of the unperturbed atomic state vectors $|F_g, m_g\rangle$ and $|F_e, m_e\rangle$:

$$|\Psi(F', m')\rangle = \sum_{F_e} \mathcal{C}_{F'F_e} |F_e, m_e\rangle, \quad (4)$$

for an excited state, and

$$|\Psi(F, m)\rangle = \sum_{F_g} \mathcal{C}_{FF_g} |F_g, m_g\rangle \quad (5)$$

for the ground state. The sums are done only on eigenvectors with the same m in zero magnetic field since the perturbation introduced by the magnetic field couples only states with the same m .

The components of the electric-dipole moment \mathbf{D} are

$$\langle \Psi(F', m') | \mathbf{D}_q | \Psi(F, m) \rangle = \mathcal{A}(\Psi(F', m'); \Psi(F, m); q) \times \left(\frac{3\pi\epsilon_0 \hbar c^3}{\omega_{eg}^3} \Gamma \right)^{1/2}. \quad (6)$$

The “modified” transfer coefficients are expressed as

$$\begin{aligned} & \mathcal{A}(\Psi(F', m'); \Psi(F, m); q) \\ &= \sum_{F_e, F_g} \mathcal{C}_{F'F_e} a(F_e, m_e; F_g, m_g; q) \mathcal{C}_{FF_g}, \quad (7) \end{aligned}$$

where $a(F_e, m_e; F_g, m_g; q)$ are unperturbed transfer coefficients having the following definition [10]:

$$\begin{aligned} a(F_e, m_e; F_g, m_g; q) &= (-1)^{1+I+J_e+F_e+F_g-m_e} \\ &\times \sqrt{2F_g+1} \sqrt{2F_e+1} \sqrt{2J_e+1} \\ &\times \begin{pmatrix} F_e & 1 & F_g \\ -m_e & q & m_g \end{pmatrix} \begin{Bmatrix} F_e & 1 & F_g \\ J_g & I & J_e \end{Bmatrix}. \quad (8) \end{aligned}$$

The parentheses and curly brackets denote, respectively, $3-j$ and $6-j$ coefficients [13]. The last two equations illustrate the fact that although the coefficient $a(F_e, m_e; F_g, m_g; q)$ may be zero for some transitions in zero magnetic field, the coefficient $\mathcal{A}(\Psi(F', m'); \Psi(F, m); q)$ will in general be nonzero in a magnetic field, thus allowing usually forbidden transitions. Moreover, transitions which were equally probable in the absence of a magnetic field, such as the $\Delta m = \pm 1$ tran-

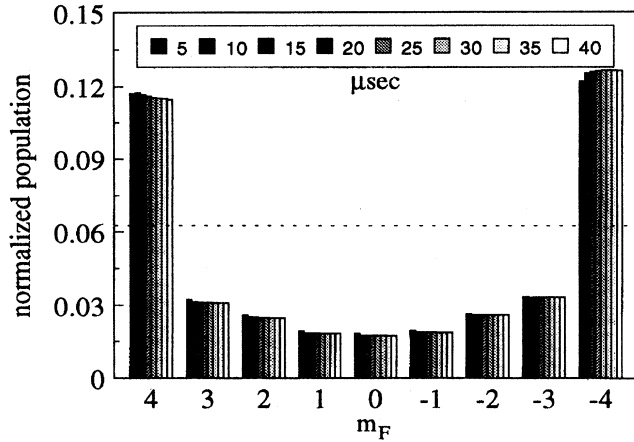


FIG. 2. The populations of the various m_F Zeeman sublevels of the $6S_{1/2}F=4$ ground state as a result of optical pumping with σ polarized light for interaction times from 5 to 40 μsec . The initial population of the levels was assumed to be Maxwell-Boltzmann, with each sublevel having 6.25% of the population, as indicated by the dashed horizontal line. The populations shown are for a laser exactly on resonance with the $6S_{1/2}F=4 \rightarrow 6P_{3/2}F'=5$ transition, with an intensity of 2.8 mW/cm^2 , a laser linewidth of 1 MHz, and in a magnetic field of 330 mG.

sitions starting from the ground-state $m=0$ sublevel, become different to first order in the field \mathbf{B} .

The optical electric field $\mathbf{E}(t)$, which is assumed to be spatially uniform over the interaction region, can be expressed as

$$\mathbf{E}(t) = E[1 + \varepsilon(t)]\{\cos[\omega t + \phi(t) + \theta]\mathbf{e}_r - \sin[\omega t + \phi(t) + \theta]\mathbf{e}_i\}, \quad (9)$$

where E is the mean amplitude, ω the mean angular frequency, and \mathbf{e}_r and \mathbf{e}_i are, respectively, the real and imaginary parts of the unit vector representing the light polarization. The random initial phase θ is uniformly distributed over the interval $]-\pi, \pi]$. The amplitude and phase fluctuations are respectively denoted by $\varepsilon(t)$ and $\phi(t)$. They are zero mean stochastic processes assumed wide-sense stationary, mean-square continuous, and uncorrelated to θ . The field can be rewritten as

$$\mathbf{E}(t) = \frac{E}{2} [\zeta(t)e^{i\omega t}\mathbf{e} + \zeta^*(t)e^{-i\omega t}\mathbf{e}^*] \quad (10)$$

in terms of the fluctuations $\zeta(t)$, which are

$$\zeta(t) = [1 + \varepsilon(t)]e^{i[\phi(t) + \theta]}. \quad (11)$$

These fluctuations contain all the stochastic processes of the optical field.

The evaluation of the time evolution of the density-matrix elements is made by substituting the representation of the electric field $\mathbf{E}(t)$, Eq. (10), and the electric-dipole moment \mathbf{D} , Eq. (6), in the analog of Liouville's equation, Eq. (1). The full development of the latter is done in Tremblay and Jacques [6]. The random nature of the laser field is taken into account by evaluating expected values of the atomic popula-

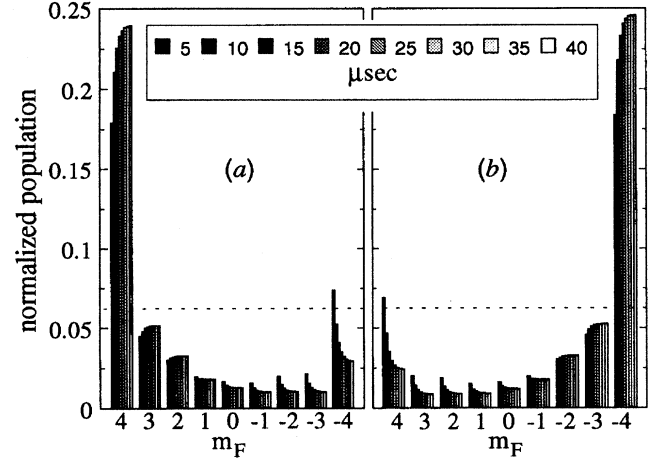


FIG. 3. The populations of the $F=4$ Zeeman sublevels as in Fig. 2 but with the laser detuned from exact resonance by (a) 1 MHz to the blue and (b) 1 MHz to the red of the $6S_{1/2}F=4 \rightarrow 6P_{3/2}F'=5$ transition. The dashed line indicates the initial population as in Fig. 2.

tions and coherences. The results of the assumption of a Lorentzian laser line shape appear as supplementary terms (proportional to laser linewidth) to the spontaneous emission and relaxation related terms. When the laser linewidth is larger than the natural linewidth of the atomic transition, the density-matrix model tends asymptotically towards a rate-equation model which includes the excitation of neighboring transitions and the effects of a static magnetic field [14]. On the other hand, for a highly monochromatic laser, the solution reduces to the standard density-matrix operator formalism [10].

The hyperfine splitting parameters used through the calculations were taken from Arimondo, Inguscio, and Violino [15] and Tanner and Wieman [16]. The complete model consists of a set of 1176 coupled linear differential equations that can only be solved numerically. It is not possible as with the rate-equation model, to obtain an analytical solution which would allow us to easily distinguish the important coherence terms responsible for the observed effects.

Numerical results

The transition probabilities for $F=4 \rightarrow F'=5$ σ polarized transitions are such that the extremum m_F Zeeman sublevels are preferentially populated. This can be seen in Fig. 2, which shows the populations of the various m_F levels as a result of optical pumping for various interaction times. The maximum interaction time chosen corresponds approximately to the maximum observable interaction time in the experiments. The initial population of the levels was assumed to be Maxwell-Boltzmann, with each sublevel thus having 6.25% or $\frac{1}{16}$ of the normalized population. The optically pumped populations shown are for a laser exactly on resonance. The slight asymmetry is explained by the change in the transition probabilities due to the static magnetic field. Detuning the laser to the red, even by as little as 1 MHz, preferentially populates the $F=4$, $m_F=-4$ state, as shown in Fig. 3(a), which in our experiment would be detected as a

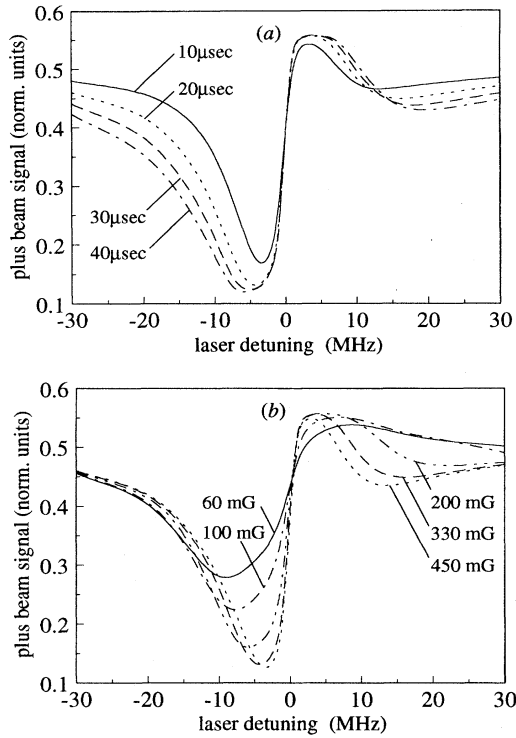


FIG. 4. The predictions of the density-matrix model for the plus beam signal as a function of laser detuning from the cycling transition resonance frequency for a σ polarized laser. Shown are (a) the population for various atom-laser interaction times at a magnetic field of 330 mG and (b) the population for various magnetic fields at an interaction time of 20 μsec . The laser intensity was 2.8 mW/cm^2 and the laser linewidth was 1 MHz.

decrease in the plus beam current. Detuning to the blue increases the population of $F=4$, $m_F=+4$ state, as shown in Fig. 3(b).

The asymmetry in the optically pumped populations for σ polarization corresponds to the “dispersion” shape of the plus beam signal as a function of the laser frequency (Fig. 4). In Fig. 4(a) we show the calculated plus beam signal in a magnetic field of 330 mG for various interaction times. While for very small detunings the dispersive shape quickly reaches its steady-state value, as the detuning from resonance increases the steady-state value of the population requires an ever increasing interaction time. In Fig. 4(b) we show the same calculated signal shown in Fig. 4(a), but now for a 20 μsec interaction time and for various magnetic fields. Both the amplitude and width of the dispersive shape changes as a function of magnetic field as will be discussed further in Sec. V.

For π polarization the transition probabilities are such that they tend to concentrate the populations in the central Zeeman sublevel, so that the optical pumping empties the extremum levels. In this case detuning of the laser to either side of resonance does not result in a significant population difference, and the extremum sublevel populations remain close to zero. The time-dependent solution for the population of the $F=4$, $m_F=-4$ state as a function of laser frequency will therefore have the shape of a dip. At resonance the popu-

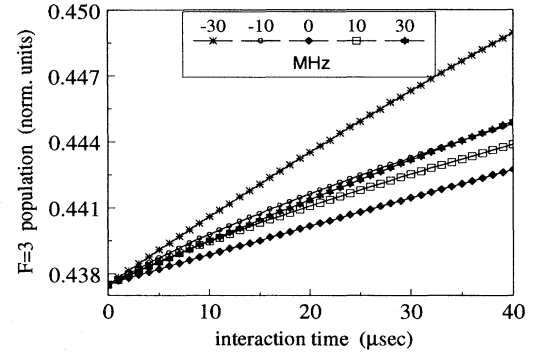


FIG. 5. The population of all the Zeeman sublevels of the $6S_{1/2}F=3$ level as a function of interaction time for a σ polarized laser, resonant or nearly resonant with the $F=4 \rightarrow F'=5$ transition. The various symbols indicate the detuning from the $F=4 \rightarrow F'=5$ resonance in MHz. The $F=3$ level population changes due to leakage to it from the laser driven $F=4 \rightarrow F'=5$ transition, thus acquiring monotonic growth as a function of interaction time. The parameters used for the calculations were as follows: laser intensity of 2.8 mW/cm^2 , laser linewidth of 1 MHz, and magnetic field of 330 mG.

lation is close to zero, and as the detuning gets larger, the population increases up to the thermal Boltzmann distribution for large detuning, which gives a population of 6.25%.

The density-matrix model used for this calculation takes into account the population leakage to and from levels very far off resonance from the laser. There are two causes of leakage: the first is due to the finite linewidth of both the laser and the atomic transition. For our experiment, the predominant leakage transition due to this effect is the $F=4 \rightarrow F'=4$ transition. The second cause is due to state mixing by the magnetic field which thus allows usually forbidden transitions. The predominant leakage transition due to this effect is the $F=3 \leftarrow F'=5$, which occurs predominantly as a relaxation process. For a magnetic field of 330 mG the spontaneous emission rate for this transition is $10^{-6}\Gamma$. Since the $F=3$ level is not subjected to repumping in this experiment, it acts as a trap, as shown by the monotonic growth of the population of $F=3$ with interaction time (Fig. 5). Here we can see that the $F=3$ population has a steady, albeit very slow, growth, and for very long interaction times, all the population would eventually concentrate in the $F=3$ state. The leakage rate is larger for red detunings from the $F=4 \rightarrow F'=5$ resonance since then the laser is closer to the $F=4 \rightarrow F'=4$ transition. Very near the cycling transition resonance, the leakage rate has a local minimum, since the $F=4$ ground-state population is depleted due to the strong and preferential pumping between the cycling transition levels.

Although the effects of leakage are always present, for laser linewidths of the order of 1 MHz, low magnetic fields and short laser-atom interaction times, they are negligible, as shown in Fig. 6. In the figure we plot the calculated population of the plus beam ($F=4$, $m_F=+4, \dots, -3$) as well as the calculated population of the $F=4$, $m_F=-4$ Zeeman sublevel subtracted from 9/16, as a function of the laser frequency. Since all the populations are normalized so that the total ground-state population ($F=3$ and $F=4$) equals 1,

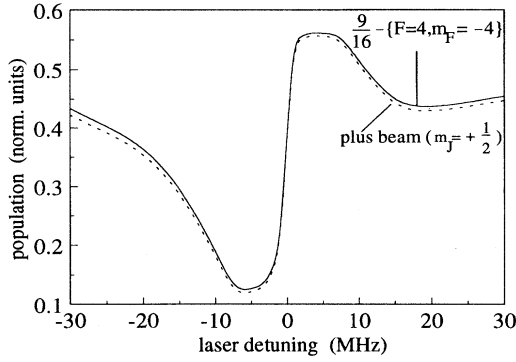


FIG. 6. Calculated populations of the plus beam ($m_j = 1/2$) and the population of the Zeeman sublevel ($F=4$, $m_F = -4$) as a function of laser detuning. The latter is subtracted from $9/16$, the nominal population of the total $F=4$ state [$9/16 -$ the ($F=4$, $m_F = -4$) population], in order to display the small effects of leakage to the $6S_{1/2}F=3$ level. The difference between the two curves is the population leakage as a function of laser detuning from the cycling transition frequency. Without any leakage to $F=3$, the two curves would be identical. The parameters used for the calculation were the same as in Fig. 5 and are for an interaction time of $40 \mu\text{sec}$. For shorter interaction times the difference between the two curves is even smaller.

$9/16$ is the nominal Boltzmann population of the $F=4$ state before the optical pumping. To demonstrate that the difference between the two curves in the figure is just equal to the leakage from the $F=4$ to the $F=3$ state, we first note that the plus beam population is equal to $[1 - \{\text{the minus beam population}\}]$. If there would be no leakage to $F=3$, the populations of the $F=3$, $m_F = +3, \dots, -3$ would be a constant equal to $7/16$. If there is leakage to $F=3$ then $[1 - \{\text{the minus beam population}\}]$ is equal to $[1 - \{(7/16) + (F=4, m_F = -4) + (\text{leakage})\}]$ which is equal to $[9/16 - (F=4, m_F = -4) - (\text{leakage})]$. Thus the difference between the plus beam population and $[9/16 - (F=4, m_F = -4)]$ is the leakage from $F=4$ to $F=3$, and as shown in the figure, this difference is negligibly small.

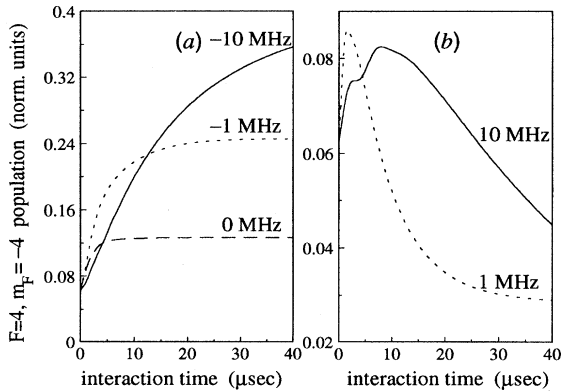


FIG. 7. The evolution of the population of the $F=4$, $m_F = -4$ level population as a function of interaction time for (a) a laser resonant and with negative (red) detunings and (b) positive (blue) laser detunings in MHz. The calculations are for $B=330 \text{ mG}$, σ polarization, laser intensity of 2.8 mW/cm^2 , and linewidth of 1 MHz .

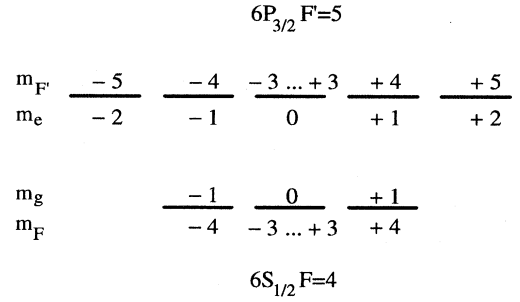


FIG. 8. Energy-level diagram for the Cs cycling transition, showing the simplification made for the 8 level rate-equation model. The central seven Zeeman sublevels in both upper and lower states have been lumped into a single effective sublevel.

The time evolution of the population of the $F=4$, $m_F = -4$ sublevel, for σ polarization, is typical of a multi-exponential decay curve (Fig. 7). The numerous contributions of the many single-photon and multi-photon paths towards and away from the $m_F = -4$ sublevel makes the comprehensive understanding of all the exponential components difficult. For very short times all the curves, for either positive or negative laser detuning, show an initial population growth, due to the redistribution of population towards the extreme Zeeman levels, $m_F = \pm 4$. This process, the result of which is shown in Fig. 2, is very efficient due to the large transition probabilities and the efficient absorption and stimulated emission. After a few microseconds, the population due to this process reaches a quasiequilibrium and further population changes occur in response to the coherence terms. For these terms, depending on the laser detuning and the magnetic field, a number of time scales become important as can be seen in the structure of the time dependence in Fig. 7. As expected, equilibrium populations are reached much more quickly for small detunings ($1-10 \text{ MHz}$) from line center. For larger detunings the time scale becomes very long.

IV. RATE-EQUATION MODEL

The rate-equation model we use considers only the sublevels involved in the cycling transition and specifically ignores the possibility of population “leakage” to the $6S_{1/2}F=3$ ground state. This assumption is justified on the basis of the full density-matrix calculation, as outlined above, which shows that the population of the $F=3$ ground state remains practically unchanged under a broad range of experimental conditions, including the parameters used in our experiments. This assumption greatly simplifies the rate-equation model, and makes it amenable to interpretation.

The model is solved numerically for the case of the Cs D_2 cycling transition, thus resulting in 20 equations for the 20 sublevels. We also solved the rate equations for a much reduced system with as few equations (sublevels) as possible, that still retains the essential features of the full rate-equation model. For the reduced system we assumed that all sublevels with $|m_F| \leq 3$ can be lumped into one effective central sublevel. Thus the reduced system, shown in Fig. 8, consists of 3 sublevels in the ground state: $m_g = -1, 0, 1$ and 5 sublevels in the excited state: $m_e = -2, \dots, +2$ thus yield-

ing a total of 8 sublevels instead of the 20 sublevels actually present for the Cs cycling transition. Numerically we find that the overall behavior of both the reduced and full system are the same. However, because the reduced system can be solved analytically, it allows us to obtain an analytic expression for the functional shape of the population of the extremum levels. The absolute numerical values of the populations obtained from such a reduced system of sublevels are clearly of no relevance since the oscillator strengths used for the lumped sublevels are fictional.

The 20 (or 8) equations that have to be solved in the rate equation model have the form

$$\begin{aligned} \frac{dN_{F',m'}}{dt} = & \sum_q (N_{F,m-q} W_{F,m-q \rightarrow F',m'} \\ & - N_{F',m'} W_{F',m' \rightarrow F,m-q}) \\ & - N_{F',m'} \sum_{k=(m-1)}^{m+1} A_{F',m' \rightarrow F,k}, \end{aligned} \quad (12)$$

$$\begin{aligned} \frac{dN_{F,m}}{dt} = & -N_{F,m} \sum_q W_{F,m \rightarrow F',m'+q} \\ & + \sum_q N_{F',m'+q} W_{F',m'+q \rightarrow F,m} \\ & + \sum_{k=(m'-1)}^{m'+1} N_{F',k} A_{F',k \rightarrow F,m}, \end{aligned} \quad (13)$$

where selection rules dictate that $m=m'$. The range of m' values for $F'=5$ is $m' = +5, \dots, -5$ in Eq. (12), (or for $F'=2$, $m' = -2, \dots, +2$ in the reduced system) and for $F=4$, $m = +4, \dots, -4$ in Eq. (13) (or for $F=1$, $m = -1, 0, +1$ in the reduced system). The polarization vector index is q with $q = \pm 1$ for σ polarization, and $q=0$ for π polarization. $N_{F,m}$ is the population of the $\{F:m\}$ state, $A_{F,m \rightarrow F',m'}$ is the spontaneous transition rate with $a_{F,m \rightarrow F',m'}^2 = \tau A_{F,m \rightarrow F',m'}$ where $a_{F,m \rightarrow F',m'}$ is defined in Eq. (8) and τ is the transition lifetime. $W_{F,m \rightarrow F',m'}$ is the induced transition rate derived from the convolution of the laser line shape and the line shape for the transition between the Zeeman sublevels:

$$\begin{aligned} W_{F,m \rightarrow F',m'} = & \frac{3\lambda^3 I_L}{8\pi^2 h c} A_{F,m \rightarrow F',m'} \\ & \times \int_{-\infty}^{\infty} g_{F,m \rightarrow F',m'}(\nu) \rho_L(\nu) d\nu. \end{aligned} \quad (14)$$

λ is the laser wavelength, h is Planck's constant, c the speed of light, I_L the laser intensity in W/m^2 (for σ polarization I_L should be multiplied by a factor of 1/2 due to the fact that σ polarization consists of equal amounts of $\sigma^{(+)}$ and $\sigma^{(-)}$ components), and $g(\nu)$ and $\rho_L(\nu)$ are the atomic transition and laser line shapes, respectively. We take both line shapes to be normalized Lorentzians, and with this assumption Eq. (14) becomes

$$\begin{aligned} W_{F,m \rightarrow F',m'} = & \frac{3\lambda^3 I_L}{8\pi^2 h c} \left\{ \frac{(\gamma + \gamma_L)}{(\nu_L - \nu_{F,m \rightarrow F',m'})^2 + (\gamma + \gamma_L)^2} \right\} \\ & \times A_{F,m \rightarrow F',m'}, \end{aligned} \quad (15)$$

where 2γ and $2\gamma_L$ are the FWHM of the atomic and the laser linewidths in Hz.

A. Solution for the extremum levels — σ polarization

For the 8 level reduced system we obtain an analytic solution for the steady-state extremum level populations, provided we make a number of assumptions: (i) as in the density-matrix model, $W_{F,m \rightarrow F',m'}$ is assumed to be constant as the atom traverses the laser beam (i.e., we assume that the laser beam profile is uniform, implying that I_L has no spatial dependence), (ii) the laser intensity is sufficiently low so that the stimulated rates are much smaller than the spontaneous rates, and (iii) the relative transition probabilities between the states are independent of magnetic field, and can be evaluated from Eq. (8). In order to simplify the notation we define $T_{m,m'} = T_{-m,-m'} \equiv a_{F,m \rightarrow F',m'}^2$; $W_{m,m'} \equiv W_{F,m \rightarrow F',m'}$; $\nu_{m,m'} \equiv \nu_{m'} - \nu_m$ is the energy-level difference (in Hz); $\Delta_{m,m'} \equiv \nu_L - \nu_{m,m'}$ is the laser detuning and ν_L is the laser frequency. The population of the ground-state $m = -1$ sublevel is then given by

$$\begin{aligned} N_{g,-1} = & \left(1 + \alpha \frac{W_{-1,0}}{W_{1,0}} \right. \\ & \left. + \left\{ \frac{(1 - \alpha^2) \{W_{-1,0}/W_{1,0}\} + \beta \{W_{-1,0}/W_{0,-1}\}}{\{W_{0,1}/W_{0,-1}\} + \alpha} \right\} \right)^{-1}, \end{aligned} \quad (16)$$

$$\alpha = (1 - T_{1,0})/T_{1,0}, \quad \beta = T_{0,0}/(T_{1,0}T_{1,1}), \quad (17)$$

which can be further simplified to

$$\begin{aligned} N_{g,-1} = & \frac{1}{Q} + \frac{R}{Q^2} \frac{(\Delta_{0,1} + f_p)}{(\Delta_{0,1}^2 + \gamma_T^2)} - \frac{(4f_s + K)}{Q^2} \\ & \times \frac{(\Delta_{-1,0} + \{[4f_s^2 + K(f_s + f_p)]/2\}/(4f_s + K))}{(\Delta_{-1,0}^2 + \gamma_T^2)}, \end{aligned} \quad (18)$$

where

$$\begin{aligned} Q = & 2 + T_{0,0}T_{1,0}/(T_{1,1}T_{0,1}), \\ R = & 4f_p \{2T_{1,0} + T_{1,0}^2 T_{0,0}/(T_{1,1}T_{0,1}) - 1\}, \\ K = & 2(f_s + f_p)T_{0,0}T_{1,0}/(T_{1,1}T_{0,1}), \\ \gamma_T = & (\gamma + \gamma_L), \end{aligned} \quad (19)$$

and f_s, f_p are the ground-state and excited-state sublevel Zeeman splittings (in Hz). The first term in Eq. (18) is a

constant, but the second and third terms result in a dispersive shape, as a function of laser detuning, Δ , having the form $\Delta/(\Delta^2 + \text{const})$. The sign of R depends on the sign of $(T_{1,0}^2 - T_{1,1}T_{0,1})$ and for the cycling transition R is negative, so both the second and third terms in Eq. (18) have the same sign. The frequency separation between the zero crossings of the two dispersive shapes is of order f_s , and in small magnetic fields (as in our case), $\gamma_T \gg f_s$, so that the individual dispersive shapes are indistinguishable.

The source of the dispersive shape, as can be seen in Eq. (16), is the term with the form $W_{m,m'}/W_{n,n'}$. These terms represent the ratio between two slightly separated Lorentzians and thus result in a dispersionlike function. Increasing the magnetic field increases the Zeeman splitting, i.e., the separation between the Lorentzians increases, so the final dispersive amplitude can be expected to grow with magnetic

field. Physically, such ratios appear due to the competition between the optical pumping of two slightly displaced transitions.

B. Solution for the central levels — σ polarization

An interesting result of the reduced model is that the central level population, with $m_g = 0$, has a double-peaked line shape. This implies that a maximum in the population difference between the $\Delta m_F = 0$ clock levels of Cs (the “atomic clock levels”), $(N_{4,0} - N_{3,0})$, is obtained by optical pumping a few MHz away from exact resonance with the cycling transition, $F = 4 \rightarrow F' = 5$. This is shown as the inset in Fig. 9. The asymptotic analytic solution for the population of this level (with the same assumptions as were made for the populations of the extremum levels) has the form

$$N_{g,0} = A\beta - 2A^2\beta \frac{[\delta(\delta + 2f_p) + \alpha\mu(\mu + 2f_p)]\Delta_{0,0}^2 - \delta\mu(1 + \alpha)(\gamma_T^2 + f_p^2)}{\Delta_{0,0}^4 + 2(\gamma_T^2 - f_p^2)\Delta_{0,0}^2 + (\gamma_T^2 + f_p^2)^2} - 0.5(A\beta)^2\tau L + 0.5A\beta\tau\{W_{0,1} + W_{0,-1} + [(1 + \alpha)/\beta](W_{1,0} + W_{-1,0})\}, \quad (20)$$

where

$$\begin{aligned} A &= [2 + 2\alpha + \beta]^{-1}, \\ \alpha &= (1 - T_{1,0})/T_{1,0}, \\ \beta &= T_{0,0}/(T_{0,1}T_{1,1}), \\ \delta &= f_p - f_s, \\ \mu &= f_p = f_s, \\ \gamma_T &= \gamma + \gamma_L. \end{aligned} \quad (21)$$

The definition of L is

$$\begin{aligned} L &= [(1 + \alpha)/\beta](W_{1,2} + W_{-1,-2}) + \xi(W_{0,1} + W_{0,-1}) \\ &\quad + [3/(\beta T_{1,0})](W_{-1,0} + W_{1,0}), \\ \xi &= 1 + \frac{T_{1,1}(T_{0,1}T_{1,0} - T_{0,1} - 2T_{1,0})}{T_{0,0}T_{1,0}(T_{1,0} - 1)}. \end{aligned} \quad (22)$$

The first term in Eq. (20) is a constant. The second term is a polynomial of second order ($a\Delta^2 - b$) divided by polynomial of fourth order ($\Delta^4 + g\Delta^2 + h$) which gives a double-peaked shape. The third and the fourth terms have Lorentzian shapes, with each containing several $W_{m,m'}$ Lorentzians, slightly shifted from one another with a shift of order f_s . In small magnetic fields these shifts are negligible compared to the width of the Lorentzian, γ_T , and thus these terms contribute a Lorentzian shape. The total line shape is thus a Lorentzian with a double-peaked line center.

For comparison with this result we show in Fig. 9 the result for the population difference of the two ground-state $m_F = 0$ sublevels, $(N_{4,0} - N_{3,0})$, as obtained from the full density-matrix calculation. Shown are calculations for $B = 60$ and 330 mG, and interaction times 10 and 40 μsec for each magnetic field. As we mentioned above, the leakage to the $F = 3$ levels is negligible, and the population of the $m_F = 0$ sublevel of the $F = 3$ state is approximately a constant. Thus the shape shown in Fig. 9 represents changes in the population of the $6S_{1/2}F = 4$, $m_F = 0$ level, which, as in

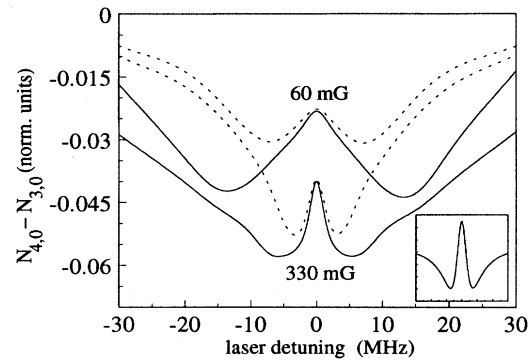


FIG. 9. Population difference, $(N_{4,0} - N_{3,0})$, of the ground-state hyperfine levels (the “clock levels”) with $m_F = 0$, calculated from the density-matrix model in magnetic fields of 60 and 330 mG and for interaction times of 10 (dashed line) and 40 (solid line) μsec with a laser tuned to the $6S_{1/2}F = 4 \rightarrow 6P_{3/2}F' = 5$ transition with linewidth of 1 MHz and $I = 2.8$ mW/cm². The shape of the population difference is determined mostly by the population of the $6S_{1/2}F = 4$, $m_F = 0$ level, because of the negligible effects of leakage to the $F = 3$ levels. The inset shows the asymptotic solution for the same population difference obtained from the 8 level rate-equation model for a magnetic field of 330 mG.

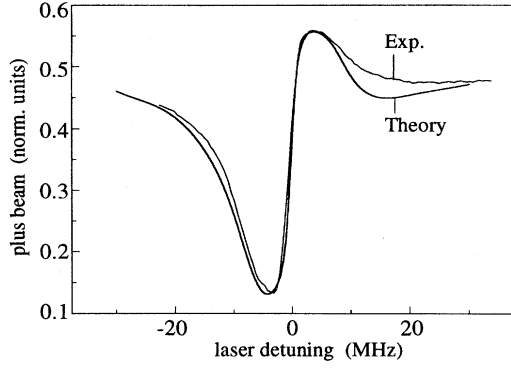


FIG. 10. Calculated and experimentally observed plus beam signal for σ polarization in normalized units (where 1 is the total population of all the ground states of the Cs hyperfine levels). The laser used was a stabilized HLP-1400 diode laser with laser intensity of 2.8 mW/cm^2 , the magnetic field was 330 mG, and the atom-laser interaction time was $\sim 20 \mu\text{sec}$.

the rate-equation model, has the characteristic double-peaked shape.

C. Solution for the extremum levels — π polarization

The analytic solutions for π polarization are much simpler since the laser couples only pairs of Zeeman sublevels possessing the same m_F quantum number. The steady-state solution for the extremum levels is

$$N_{g,-1} = M \left[1 + 2\delta \frac{\Delta_{-1,-1} - \{\delta(0.5 + M) + (P - U)I_L / (2\delta)\}}{\Delta_{-1,-1}^2 + \gamma_T^2} \right], \quad (23)$$

where I_L is the laser intensity, δ , γ_T , and $\Delta_{-1,-1}$ are defined as in Eq. (21), and

$$M = [2 + T_{0,-1}T_{-1,-1} / (T_{-1,0}T_{0,0})]^{-1},$$

$$P = M \left(2 + 2 \frac{T_{0,-1}}{T_{-1,0}} - \frac{T_{0,-1}T_{-1,-1}}{T_{-1,0}T_{0,0}} \right) \frac{\lambda^3 \gamma_T T_{-1,-1}}{6 \pi^3 \hbar C}, \quad (24)$$

$$U = (T_{-1,-1} + T_{0,-1}) \frac{\lambda^3 \gamma_T T_{-1,-1}}{6 \pi^3 \hbar C}.$$

The parameter U is included here to describe the contribution of the decay of the atoms left in the excited states after the interaction with the laser. Since for π polarization the population tends to concentrate in the central Zeeman sublevels, leaving close to zero population in the extremum levels, relaxation from the excited states can be a significant source of extremum level population. For σ polarization, however, this relaxation contribution is relatively small and it was included only in the numerical calculations.

For π polarization, the steady-state population of the $F=4$, $m_F=-4$ sublevel, as given by Eq. (23), is also a dispersive function, but because the population of the extremum levels is very close to zero, the dispersive amplitude is very small and thus it cannot be resolved. As it was for σ

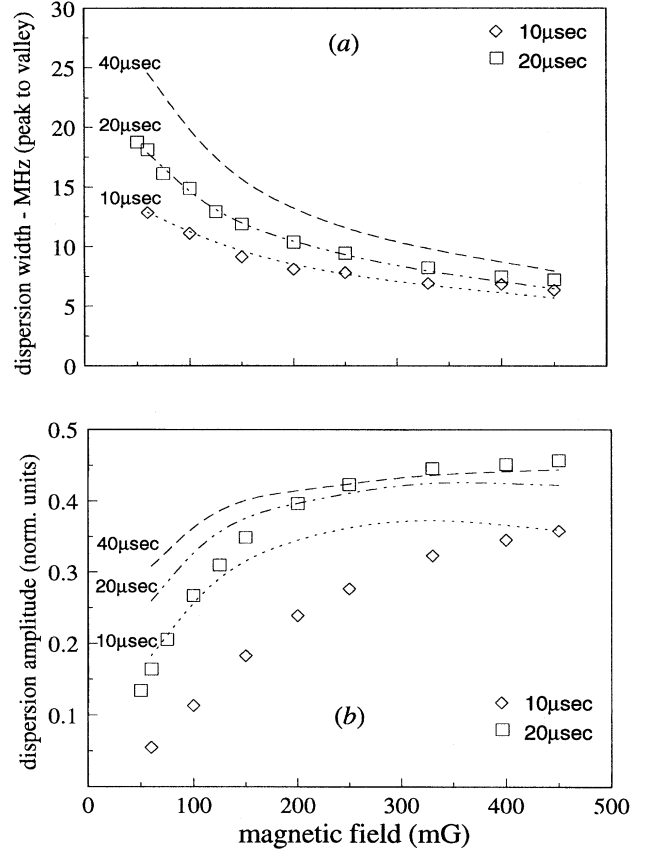


FIG. 11. The calculated and observed peak-to-valley width (a) and amplitude (b) of the dispersive shape for σ polarization as a function of magnetic field for several interaction times. The $10\text{-}\mu\text{sec}$ interaction time data were measured with an SDL-5402, stabilized diode laser, and the $20\text{-}\mu\text{sec}$ interaction time data were measured with a stabilized, HLP-1400 diode laser.

polarization, the population of the extremum sublevels for π polarization also depends on the interaction time of the laser with the atoms. Steady state is reached quickly near line center, where this population goes to zero, and as the laser is detuned from line center the depletion of the population from these levels takes much longer. Thus for a given interaction time the laser frequency dependent population appears as a dip at line center, as we have already explained in the numerical results section of the density-matrix model.

V. DISCUSSION

A. σ polarization

In Fig. 10 we show the plus beam signal, as calculated using the density matrix, for σ polarization, including the relaxation from the excited states after the interaction with the laser. Also shown is the experimental data for σ polarization, with a laser intensity of 2.8 mW/cm^2 and a magnetic field of 330 mG. The experimental data is scaled to normalized population units, i.e., the measured plus beam signal is taken to be 1/2 when the laser is far from resonance with any of the Cs transitions. The laser used to obtain this data was a

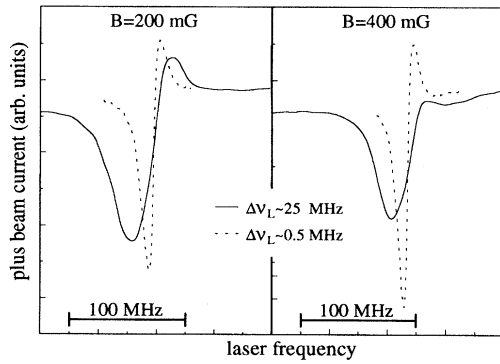


FIG. 12. The dispersive signal for two different laser linewidths of 0.5 (dashed line) and 25 MHz (solid line), each for a magnetic field of 200 and 400 mG. The laser interaction time for all the data was 20 μ sec.

stabilized HLP-1400 diode laser, and the laser-atom interaction time, as determined by the spot size of the laser at the atomic beam, was ~ 20 μ sec. Moving the Nb hot wire so that it measures the minus beam, yields a complementary signal which, as expected, is an exact mirror image of the plus beam signal. In calculating the dispersive shape we used the experimentally measured parameters with no free adjustable parameters.

The width of the dispersive line shape as well as its amplitude depend on magnetic field and this is demonstrated in Figs. 11(a) and 11(b). Calculations (dotted lines) are shown for interaction times up to 40 μ sec while the experimental interaction times are 10 and 20 μ sec. Experimentally the maximum observable interaction time is ~ 30 μ sec, which corresponds to atoms with a speed of 100 m/sec and a laser beam diameter of ~ 3 mm. For low magnetic fields both the width and the amplitude depend strongly on the interaction time. As we had already seen in Fig. 7, the time required to reach equilibrium is a strong function of laser detuning. As the dispersive shape broadens for low magnetic fields, the maximum and minimum of the dispersion curve are at frequencies further detuned from resonance [see Fig. 4(b)], where the time required to reach steady state is longer. Thus the role of the interaction time for low magnetic fields becomes more significant. The agreement of the calculation and experiment for the width of the dispersion is excellent.

The agreement is not as good for the dispersive amplitude, especially for low magnetic fields. One cause of this discrepancy is due to the sensitivity of the amplitude to small deviations from perfectly aligned polarization of the laser to the magnetic field, which is particularly true at low fields where the quantization axis is less well defined by the Helmholtz coils and parasitic, residual magnetic fields play a role. The misalignment of the polarization axis from the magnetic quantization axis results, in general, in a situation for which the polarization state of the light is mixed (neither pure σ or π). Therefore, for low magnetic fields, the polarization of the laser is not well defined and this can easily lead to a reduced dispersion amplitude. For fields larger than ~ 100 mG, however, and the degree of polarization axis to magnetic field axis alignment in our experiments (about 5°), this results in small errors. We have not clearly identified the

source of the discrepancy at fields higher than 100 mG and for short interaction times. One possibility is that the amplitude of the dispersion is more sensitive to the precise form of the laser line shape and to the statistics of the laser fluctuations.

The agreement of the density-matrix calculation with experimentally observed dispersive width and amplitude is in strong contrast with the results obtained from the rate-equation model, which provided only a qualitative explanation of the data [7]. We thus infer that the coherences, especially the optical and Zeeman coherences, which are inherent in the density-matrix model, are responsible for the much improved agreement between theory and experiment. We are not able, however, to specify which coherence term or terms are most directly responsible for the redistribution of the populations.

A clear demonstration of the importance of the coherence terms in the population redistribution can be seen by considering the increase in the relaxation rate of the coherences with laser linewidth. The linewidth of the laser enters the density-matrix calculations as part of the relaxation terms for the coherence elements of the density matrix (see Table I of Ref. [6]). Thus by looking at the dispersive shape for different laser linewidths we expect to observe a weakening of the effect as the laser linewidth increases. For very broad laser linewidths the solution approaches asymptotically the rate-equation solution. This is shown in Fig. 12, which contains four different experimental plots of the dispersive shape, for two different laser linewidths, of 0.5 and 25 MHz, at two different magnetic fields, 200 and 400 mG, respectively. At a 200 mG field the dispersion signal amplitudes for both laser linewidths are comparable. For even lower fields (not shown in the figure) the amplitudes become even more nearly equal. The widths of the dispersion signals, however, are different, as can be expected, due to the differences in laser linewidth. As the magnetic field is increased from zero up to about 200 mG, the amplitude of the dispersive shape, for both laser linewidths, grows in a manner similar to that shown in Fig. 11. For a further increase in magnetic field, however, the Zeeman sublevel separations become significant, and only the narrow linewidth laser continues to maintain strong coherences. Thus the dispersive shape for the broad laser disappears and we observe a line shape for the population redistribution which is similar to what would be expected from a time-dependent rate-equation analysis. A similar disappearance of coherence has been observed in other experiments [2,17] for lasers with a linewidth exceeding 30 MHz and a magnetic field greater than 300 mG. Further increasing the magnetic field results in a total disappearance of the dispersive shape for the broad laser, while for the narrow linewidth laser the narrow dispersive shape persisted up to the highest fields we studied, ~ 500 mG. Based on calculations, the dispersive shape for even very narrow linewidth lasers disappears, if the magnetic field is increased significantly.

B. π polarization

For π polarization, only optical coherences are established by the laser without Zeeman coherences in either the excited or ground state. Thus the theoretical models for this polarization are much simplified and it is reasonable to expect that the density-matrix and rate-equation models should

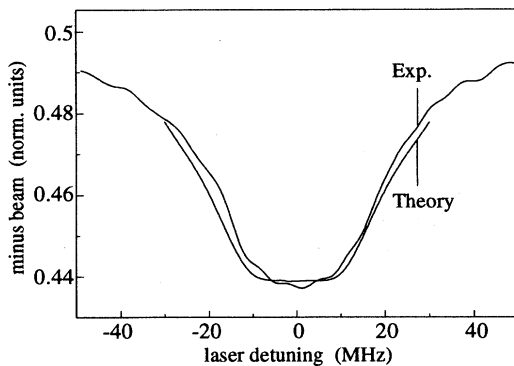


FIG. 13. Observed and calculated minus beam signal in normalized units for π polarization. The theoretical plot was obtained using the density-matrix formalism. The parameters for the theory are taken from the experiment and are as follows: a laser intensity of 2.8 mW/cm^2 , interaction time of the atoms with the laser of $\sim 12 \text{ } \mu\text{sec}$, and a magnetic field of 330 mG .

yield nearly identical results. This is indeed the case and for this polarization the shape of the calculated plus beam signal is a peak, while the minus beam is predicted to have a valley shape. The comparison of the experimental minus beam signal to the density-matrix prediction is shown in Fig. 13, demonstrating good agreement. The signal in this case is almost completely independent of magnetic field. The signal does depend on the laser linewidth and the interaction time as expected from both the density-matrix and rate-equation calculations. For the experimental plus beam signal we observed an additional dispersion shaped feature on top of the theoretically expected peak. This feature [7] is completely independent of magnetic field, and owes its origin to effects not discussed in this paper [18].

VI. CONCLUSIONS

We have found, both experimentally and theoretically, that σ polarized laser light causes a dispersive redistribution in the population of the extremum Zeeman sublevels of a nondegenerate multilevel system. The dispersive line shape is a general phenomenon, and can be observed even if the splitting of the levels is orders of magnitude smaller than the linewidth of the laser and/or the linewidth of the atomic transition. This implies that the dispersive shape is not due to changes in the different transitions rates as a function of laser detuning. The population redistribution can be qualitatively predicted and explained by a rate-equation model, but the model fails greatly in making quantitative predictions. A full density-matrix model, which takes into account all the laser-induced atomic coherences, predicts the effect quantitatively, and correctly describes the dependence of the populations on laser detuning, laser polarization, interaction time, and magnetic field. Similarly, the calculations show that the population of the central Zeeman sublevel ($m=0$), which is used in Cs clocks, has a double-peaked line shape, with a minimum population occurring for off-resonant laser pumping. For a π polarized laser the transition probabilities are such that the optical pumping empties the extremum levels. Therefore, both experiment and calculation show that the time-dependent solution for the extremum level populations decreases as resonance is approached.

ACKNOWLEDGMENTS

Two of us (Y.N. and M.R.) acknowledge support of this research by the German-Israel Science Foundation. Discussions with Professor T. Hansch and his group were most valuable.

-
- [1] M. O. Scully and S. Zhu, *Phys. Rev. Lett.* **62**, 2813 (1989); M. O. Scully, *ibid.* **67**, 1855 (1991); E. S. Fry *et al.*, *ibid.* **70**, 3235 (1993); A. Nottelmann, C. Peters, and W. Lange, *ibid.* **70**, 1783 (1993); U. Rathe, M. Flieschauer, S.-Y. Zhu, T. Hansch, and M. O. Scully, *Phys. Rev. A* **47**, 4994 (1993); A. Imamoglu, J. E. Field, and S. E. Harris, *Phys. Rev. Lett.* **66**, 1154 (1991).
 - [2] G. Théobald, N. Dimarcq, V. Giordano, and P. Cerez, *Opt. Commun.* **71**, 256 (1989).
 - [3] V. S. Smirnov, A. M. Tumaikin, and V. I. Yudin, *Zh. Eksp. Teor. Fiz.* **96**, 1613 (1989) [*Sov. Phys. JETP* **69**, 913 (1989)].
 - [4] G. Orriols, *Nuovo Cimento B* **53**, 1 (1979).
 - [5] R. J. McLean, R. J. Ballagh, and D. M. Warrington, *J. Phys. B* **19**, 3477 (1986).
 - [6] P. Tremblay and C. Jacques, *Phys. Rev. A* **41**, 4989 (1990).
 - [7] Y. Nafcha, D. Albeck, and M. Rosenbluh, *Phys. Rev. Lett.* **67**, 2279 (1991).
 - [8] Y. Nafcha, S. Whitman, D. Albeck, and M. Rosenbluh, *Opt. Commun.* **90**, 51 (1992).
 - [9] The atomic clock tube is a modified commercial device manufactured by TFL Ltd., Jerusalem, Israel.
 - [10] É. de Clercq, M. de Labacherrie, G. Avila, P. Cerez, and M. Têtu, *J. Phys. (Paris)* **45**, 239 (1984).
 - [11] J. Vanier and C. Audion, *Quantum Physics of Atomic Frequency Standards* (Hilger, Bristol, 1989), Chap. 1.
 - [12] P. Tremblay, A. Michaud, M. Levesque, S. Thériault, M. Breton, J. Beaubien, and N. Cyr, *Phys. Rev. A* **45**, 2766 (1990).
 - [13] A. Messiah, *Mécanique Quantique* (Dunod, Paris, 1972), Tome 2.
 - [14] C. Cohen-Tannoudji, in *Frontiers in Laser Spectroscopy*, 1975 Les Houches Lectures, edited by R. Balian, S. Haroche, and S. Liberman (North-Holland, Amsterdam, 1975), Vol. I, pp. 1–104.
 - [15] E. Arimondo, M. Inguscio, and P. Violino, *Rev. Mod. Phys.* **49**, 31 (1977).
 - [16] C. E. Tanner and C. Wieman, *Phys. Rev. A* **38**, 1616 (1988).
 - [17] A. Hamel, P. Petit, G. Théobald, P. Cerez, and C. Audoin (unpublished); E. de Clercq and P. Mangin (unpublished).
 - [18] The small dispersive shape seen on the plus beam signal for π polarization owes its origin to effects not discussed in this

paper and can also be observed for other polarizations, provided high laser intensities are used. For example, we were able to produce it for $\sigma^{(-)}$ polarization, on the minus beam when the laser intensity was greater than 22 mW/cm². Similarly, we were able to produce small dispersive shapes of identical symmetry superimposed on the plus beam signal when we

used σ or $\sigma^{(-)}$ polarizations with laser intensity of 45 mW/cm², and for $\sigma^{(+)}$ polarizations with a laser intensity of 6 mW/cm² or greater. The shape for $\sigma^{(-)}$ and $\sigma^{(+)}$ polarizations, as calculated by the models presented here, should be symmetric and have a simple peak or valley shape as a function of the laser frequency.